ACS APPLIED NANO MATERIALS

www.acsanm.org Article

# Electrochemical Functionalization of Selectively Addressed $MoS_2$ Nanoribbons for Sensor Device Fabrication

Martina Lihter,* Michael Graf, Damir Iveković, Miao Zhang, Tzu-Hsien Shen, Yanfei Zhao, Michal Macha, Vasiliki Tileli, and Aleksandra Radenovic*

Cite This: *ACS Appl. Nano Mater.* 2021, 4, 1076−1084 Read Online

ACCESS | Metrics & More | Article Recommendations | Supporting Information

**ABSTRACT:** Tailoring the surface properties of 2D materials, such as transition metal dichalcogenides (TMDCs), at the nanoscale is becoming essential in the fabrication of various 2D material-based nanoelectronic devices. Due to the chemical inertness of their basal plane, the surface modification of 2D TMDCs is limited to their defective sites, often requiring special treatments, such as the conversion of the TMDC from its semiconducting into its metallic phase. In this work, we show that the basal plane of a semiconducting 2D TMDC, molybdenum disulfide ($MoS_2$) can be modified electrochemically by electrografting of aryl-diazonium salt. To demonstrate the advantages of this method at the nanoscale, we perform electrografting of 3,5-bis(trifluoromethyl)benzenediazonium tetrafluoroborate on predefined $MoS_2$ nanoribbons by addressing them individually via a different electrode. The ability to selectively address individually contacted 2D layers opens the possibility for specific surface modification of neighboring 2D nanostructures by different functional groups. This method could be extended to other aryl-diazonium compounds, and other 2D semiconducting materials.

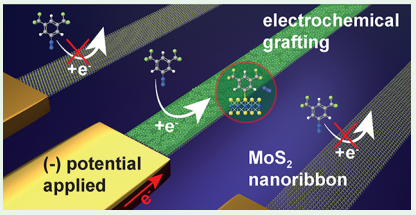


**KEYWORDS:** *2D semiconductors, molybdenum disulfide, nanoribbon, electrochemical modification, electrografting*



## INTRODUCTION

Currently, there is broad interest in 2D transition metal dichalcogenides (TMDCs) for various applications in electronics,[1,2] sensing and biosensing,[3,4] energy generation,[5,6] and energy storage.[7] This interest is motivated by a well-defined two-dimensional crystalline and electronic structure of 2D TMDCs, combined with their exceptional mechanical and chemical stability.[8] However, the chemical inertness of 2D TMDCs becomes an obstacle when it comes to tailoring their surface properties via chemical modifications.[9,10] The basal plane of 2D TMDCs is chemically inert due to the absence of dangling bonds, leaving the edges, grain boundaries, and atom vacancies as the only reactive sites for chemical modifications.[11−13] Therefore, it is rather difficult to obtain a 2D TMDC material whose surface is modified with a uniform and dense molecular layer. Constant progress in the synthesis of low-defect 2D TMDCs, driven by the need for 2D materials with controlled and reproducible properties, makes the chemical surface modification of 2D TMDCs even more challenging. The surface modification is among the easiest and most effective ways to alter the electronic and optical properties of the low-dimensional nanomaterial and tune the interactions between the material and other chemical species. Therefore, finding ways to chemically modify the surface of 2D TMDC materials with homogeneous and uniformly distributed molecular layers is one of the key steps toward practical applications of 2D TMDCs. For many of these applications (e.g., chemical sensing and biosensing, nanoelectronics or nano optics), tailoring the surface properties of the material at the nanoscale is almost an essential, which is another feature that the surface modification methods should meet in order to be successfully applied in fabrication of the 2D TMDC-based devices.

In this work, we focus on 2D molybdenum disulfide ($MoS_2$), which is a typical representative and one of the most investigated TMDCs. $MoS_2$ can exist in several polytypes among which 2H-$MoS_2$ displays semiconducting properties and is the most stable one. The majority of reported methods on surface modification of 2H-$MoS_2$ are wet chemistry methods that rely on the existence of defective sites in $MoS_2$, such as sulfur-vacancies, which can serve as anchors for molecule attachment,[14−20] or nucleation sites for basal plane modification.[21] So far, there have been only two reports on modification of 2H-$MoS_2$, which did not require preexisting defects, but utilized reactions with metal carboxylate salts[22] and with maleimides.[23] Another possible strategy that has evolved relies on the conversion of the semiconducting 2H-$MoS_2$ phase into chemically more reactive metallic 1T-phase[24−26] prior to the surface modification. This approach has shown to be effective since 1T-$MoS_2$ is more reactive due to the excess of negative charge that is introduced on its

**Received:** September 29, 2020
**Accepted:** January 19, 2021
**Published:** February 17, 2021

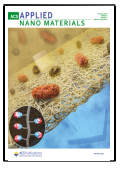




https://dx.doi.org/10.1021/acsanm.0c02628
*ACS Appl. Nano Mater.* 2021, 4, 1076−1084

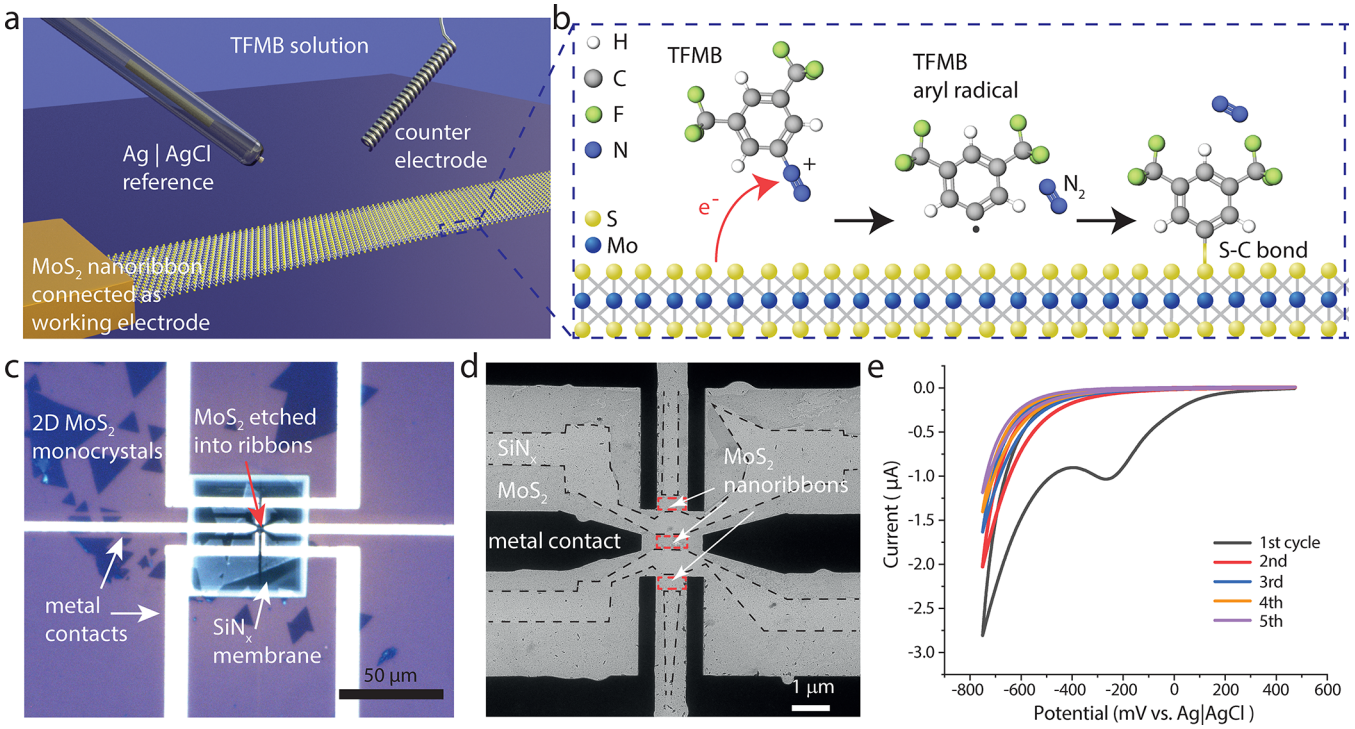


**Figure 1.** (a) A 3D illustration of the experimental setup for electrochemical grafting. $MoS_2$ is connected as a working electrode, while a AglAgCl and Pt wire serve as a reference and counter electrode, respectively. The electrodes are immersed in a solution of 5 mM 3,5-bis(trifluoromethyl)benzenediazonium tetrafluoroborate, TFMB, in acetonitrile with 100 mM tetrabutylammonium perchlorate, TBAP, which was used as a supporting electrolyte. The objects are not to scale. (b) A side-view schematic of the TFMB electrografting process onto monolayer $MoS_2$. Cathodic polarization of $MoS_2$ initiates electron transfer from $MoS_2$ to TFMB cations in solution. This process creates TFMB radicals in the vicinity of $MoS_2$, which couple to the $MoS_2$ surface forming an S−C covalent bond. (c) An optical microscopic image (top view) of a device with $MoS_2$ monolayer etched into nanoribbons. Each nanoribbon is contacted by one pair of metal contacts. The 20 nm thin $SiN_x$ membrane enables nanoribbon inspection and characterization in the transmission electron microscope. (d) A typical transmission electron microscopy (TEM) image of contacted $MoS_2$ nanoribbons on $SiN_x$ membrane (indicated in (c)). Each of the three $MoS_2$ nanoribbons is marked by a red rectangle. (e) Cyclic voltammogram of TFMB electrografting process. The electrografting was performed in a solution of 5 mM TFMB and 100 mM TBAP in acetonitrile. The $MoS_2$ nanoribbon was polarized between +450 mV and −750 mV at 50 mV $s^{-1}$ during five cycles.

surface by using organometallic compounds. This can be further enhanced with reducing agents such as metallocene.[27] However, these procedures usually involve multiple steps, which is unpractical, and a phase transition can often be incompatible with the intended application of $MoS_2$. Additionally, none of the reported methods allow the $MoS_2$ modification to be performed with spatial selectivity, especially at the nanometer scale.

An attractive alternative that could enable 2H-$MoS_2$ basal plane modification, as well as selective addressing of individual 2D crystals, is electrochemically controlled surface modification. The ultrathin $MoS_2$ layer usually behaves as an n-type semiconductor, thus by polarizing it cathodically (toward lower potentials)[28−31] the electron transfer can be facilitated from $MoS_2$ to chemical species in solution. This property could be exploited for electrochemical grafting of highly reactive species, such as aryl radicals, to the entire $MoS_2$ basal plane. Aryl radicals can be produced by electrochemical reduction of aryl diazonium salts,[32−35] and they tend to covalently bind to the surface of various materials, including graphene[36] and the $MoS_2$.[21,25] Compared to other types of grafting (e.g., spontaneous grafting, grafting controlled by heat, or by the addition of chemical agents etc.), in electrochemical grafting the reaction occurs only at the electrode surface, making it highly localized. Electrografting on $MoS_2$ has to be performed at relatively mild potentials for two reasons: first, to avoid possible metallization of $MoS_2$ that might occur at cathodic potentials,[37,38] and second, to avoid hydrogen evolution reaction on $MoS_2$, which limits the useable potential window for $MoS_2$ modification.[39] Aryl diazonium salts have an advantage that they can be reduced at relatively low cathodic potentials (around 0 V vs standard hydrogen electrode), and as well in aprotic media, which avoids hydrogen evolution reaction. The grafting process is self-limiting, meaning that the grafting terminates after deposition of a certain number of molecular layers, and it can be easily controllable.[40] Besides, differently substituted aryl diazonium salts can be easily synthesized from corresponding aniline compounds, which enables introducing different chemical groups on the surface of the 2D material. In this work, we perform electrografting of a 3,5-bis(trifluoromethyl)benzenediazonium tetrafluoroborate (TFMB) on $MoS_2$ nanoribbons fabricated from $MoS_2$ that was controllably grown by metal−organic chemical vapor deposition (MOCVD).[41] $MoS_2$ nanoribbons have previously shown as promising single-molecule sensors[4] and optoelectronic devices,[42−44] and as such hold a great promise for future nanoelectronic device applications. TFMB was chosen as a model aryl diazonium compound as it contains six fluorine atoms per molecule, which greatly facilitates the selective detection of electrografted molecules by electron probe techniques at the nanoscale.


https://dx.doi.org/10.1021/acsanm.0c02628
ACS Appl. Nano Mater. 2021, 4, 1076−1084

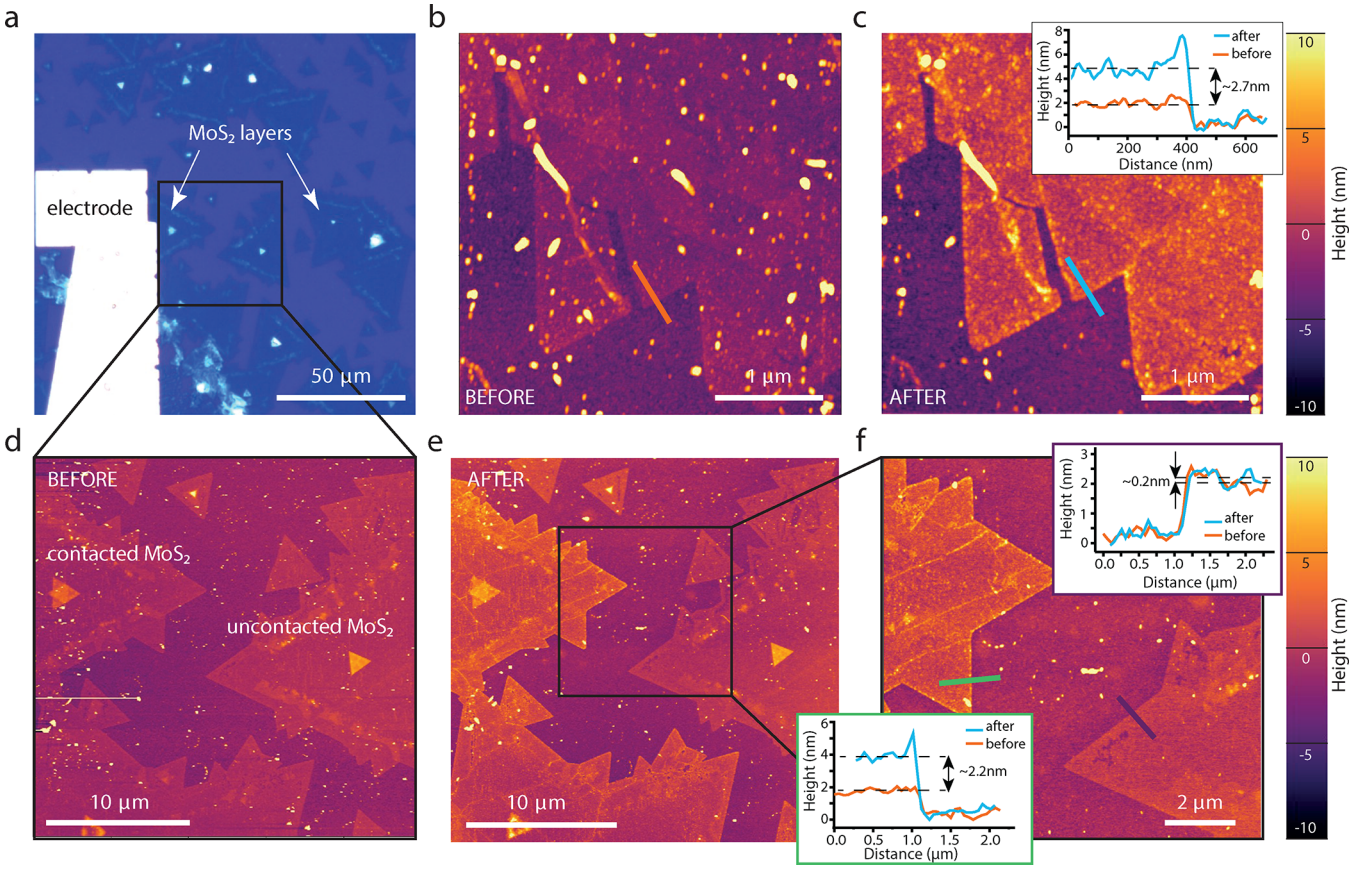


**Figure 2.** (a) Optical image of $MoS_2$ layers contacted by an electrode. The AFM image of a representative $MoS_2$ region before (b) and after (c) electrografting. The inset shows the line profile of the corresponding cross sections before and after the deposition. (d) The AFM image of the area indicated in (a) prior to electrografting, displaying mostly monolayer $MoS_2$. (e) The AFM image of the same area as in (d) after the electrografting process. (f) A close-up view of the region indicated in (e). The insets show the line profile of the two cross sections represented by a green (modified $MoS_2$) and a purple (unmodified $MoS_2$) line.

## RESULTS AND DISCUSSION

Electrografting of TFMB on 2D $MoS_2$ material was carried out by connecting $MoS_2$ as a working electrode using a three-electrode setup (Figure 1a). To investigate the applicability and selectivity of the electrografting process at the nanoscale, we used devices with electrically connected 2D $MoS_2$ nanoribbons (Figure 1c). Nanoribbons of single-layer $MoS_2$, 500 nm in width, each contacted by two metal contacts were designed on a thin $SiN_x$ membrane by nanofabrication process, described in detail in the Experimental Section. The 20 nm thin $SiN_x$ membrane is transparent to an electron beam enabling the inspection of the device and deposited layer using transmission electron microscopy (TEM) (Figure 1d). The device was immersed in a solution of TFMB in acetonitrile with tetrabuthylammonium perchlorate (TBAP) as a supporting electrolyte. In contrast to other chemical grafting procedures[21,25,26] which typically require elevated temperatures and long reaction times, we performed the reaction at low temperatures and minimized the time of exposing the device to the reaction solution (~5 min) to avoid spontaneous decomposition of aryl diazonium salt and spontaneous grafting of aryl radicals on $MoS_2$ surface. Acetonitrile was used as an aprotic solvent to prevent the hydrogen evolution on $MoS_2$. Electrografting was performed by polarizing the working electrode from +450 mV to −750 mV vs Ag | AgCl. Cathodic polarization initiates the electron transfer from $MoS_2$ surface to TFMB cation in solution, which results in generation of TFMB radical as schematically depicted in Figure 1b. The reaction can be described by $(CF_3)_2C_6H_3N_2^+ + e^- \rightarrow (CF_3)_2C_6H_3\bullet + N_2$, where $(CF_3)_2C_6H_3N_2^+$ is TFMB cation, and $(CF_3)_2C_6H_3\bullet$ a corresponding aryl radical. The radical instantly binds to the $MoS_2$ surface forming a covalent S−C bond. Figure 1e shows the cyclic voltammogram of the electrografting process. A broad peak in the first scan, around −0.3 V vs Ag | AgCl, originates from the reduction of TFMB cations.[45] The disappearance of the peak in second and subsequent cycles indicates the formation of a compact organic layer on the surface subjected to electrografting. The formed layer blocks further electron transfer between the $MoS_2$ and the aryl diazonium cations in solution,[34,45,46] which terminates the process. The formed S−C covalent bond was confirmed by X-ray photoelectron spectroscopy (XPS) (Figure S3). Details can be found in the Supporting Information (SI).

To investigate the thickness and the uniformity of the electrochemically deposited film on a larger scale, we performed atomic force microscopy (AFM) imaging on $MoS_2$ mono- and bilayers before and after electrografting process. The electrografting was performed in the same setup configuration as presented in Figure 1a, with $MoS_2$ layers electrically connected as working electrode, and reference and counter electrode immersed in the solution. Figure 2a shows an optical image of a region with several electrically connected 2D $MoS_2$ layers on which TFMB was electrografted. A part of an electrically connected $MoS_2$ layer before and after the


https://dx.doi.org/10.1021/acsanm.0c02628
ACS Appl. Nano Mater. 2021, 4, 1076−1084

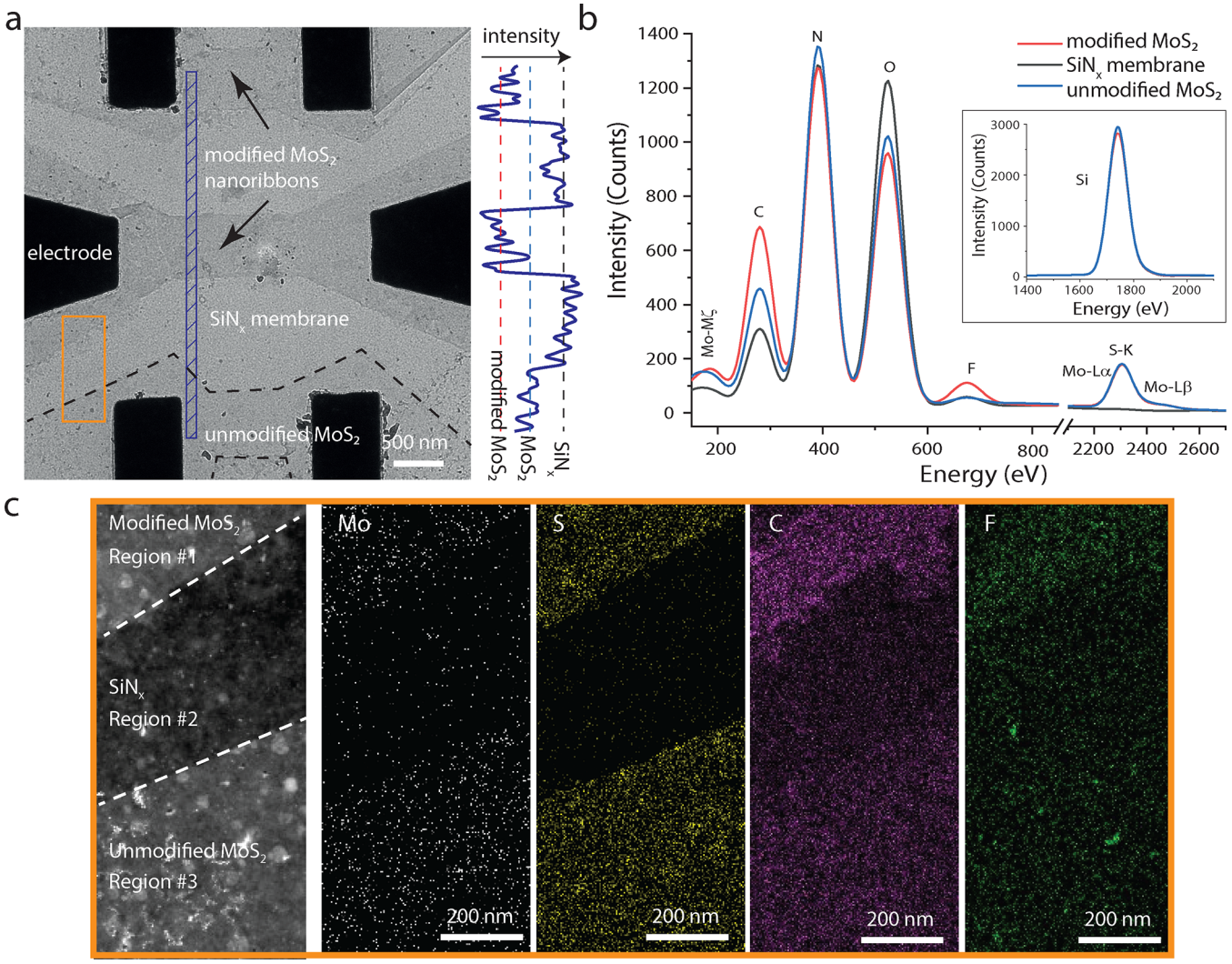


**Figure 3.** (a) A bright-field TEM (BF-TEM) image of a device with $MoS_2$ nanoribbons after the electrografting process. The upper and middle ribbon have been electrografted with TFMB (5 mM) in acetonitrile with TBAP (100 mM) as a supporting electrolyte. The electrografting was performed during five cycles from +450 mV to −750 mV at 50 $mVs^{-1}$. The line profile of the blue area is depicted next to the BF-TEM image. (b) Fitted EDX spectra obtained from three neighboring regions indicated in (a) by an orange square. The regions are more closely presented in (c, left). The modified $MoS_2$ nanoribbon (Region no. 1) exhibits an increased content of F and C originating from the electrografted TFMB molecules. F signal of the modified $MoS_2$ surface is significantly higher than the signal from the unmodified $MoS_2$ (Region no. 3) and the $SiN_x$ surface (Region no. 2). The higher level of O in Region no. 2 compared to Region nos. 1 and 3, originates from the oxygen-based reactive ion etching (RIE) of $MoS_2$. The inset shows the silicon peak. (c) The HAADF-STEM image of three regions of interest indicated by the orange rectangle in (a) from which the EDX spectra were taken, and EDX elemental maps of Mo, S, C, and F, respectively. The maps show the net (background corrected and fit) intensities of the elements present.

electrografting is shown in Figure 2b,c, respectively. The line profiles of the corresponding cross sections (Figure 2c, inset) reveal the local change in the height of 2.7 ± 0.4 nm, which corresponds to approximately four to five TFMB molecular layers (the theoretical height of TFMB monolayer is ∼6.1 Å). Figure 2d,e show a large area (indicated in Figure 2a) before and after the electrografting process, respectively. The thickness and roughness analysis at different positions can be found in SI Figure S2 and Table S1−S2. While we observe slight variations in thickness and roughness of the deposited layer, which we discuss further below, the height of unconnected $MoS_2$ layers and its surface roughness has not changed significantly. This indicates that the deposition took place only on $MoS_2$ layers that were connected to the polarized electrode. In contrast to previously reported chemical grafting on $MoS_2$,[21,25,26] which occurs on all surfaces exposed, electrochemically controlled grafting is highly localized to the cathodically polarized $MoS_2$ surface where the aryl radicals are produced. The spatial selectivity of the deposition is in this case limited by diffusion path length of the radicals, $l$, which depends on their diffusion coefficient, D, and the half-life, $\tau$, via: $l = \sqrt{D \times \tau}$. The values for $D$ and $\tau$ of aryl radicals are usually on the order of $10^{-6}$ $cm^2$ $s^{-1}$[47] and microseconds,[48] respectively. Thus, the estimated value of diffusion path length for aryl radicals is below 100 nm, indicating that the reaction layer around $MoS_2$ is extremely thin, resulting in high spatial selectivity of the electrografting method.

Figure 2f shows that the deposited layer thickness increases near the edges and grain boundaries, which can be attributed to two effects. One of them is the hemispheric diffusion at the edges, which increases the flux of TFMB cations at the edges of $MoS_2$. The second one is the higher electron transfer rate


https://dx.doi.org/10.1021/acsanm.0c02628
ACS Appl. Nano Mater. 2021, 4, 1076−1084

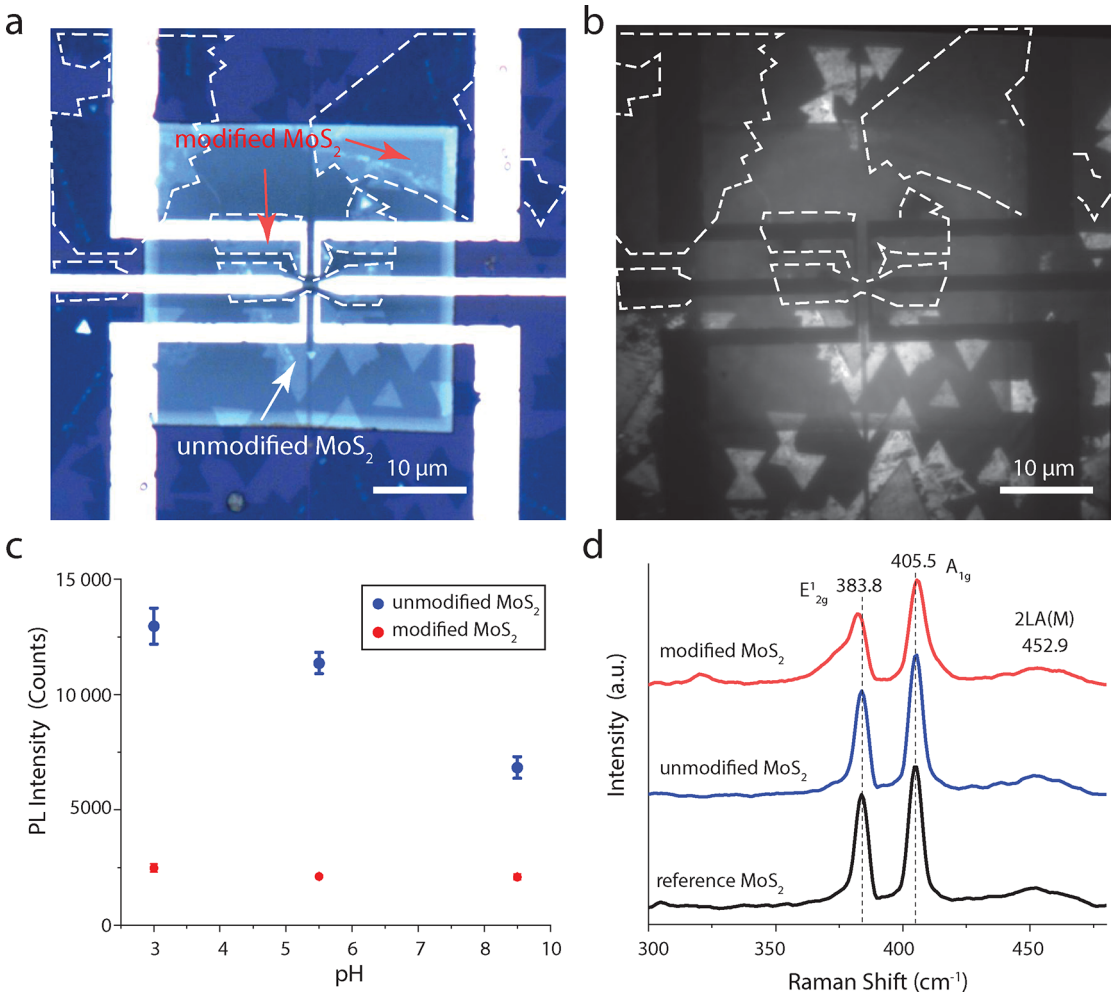


**Figure 4.** (a) An optical image of a device with $MoS_2$ nanoribbons after the electrografting process. The $MoS_2$ in contact with the upper and the middle electrodes (marked by white dashed lines) has been electrografted with TFMB (5 mM) in acetonitrile with TBAP (100 mM) as a supporting electrolyte. The electrografting was performed during five cycles from +450 mV to −750 mV at 50 $mVs^{-1}$. (b) PL image of the same region as in (a) in DI water (pH 5.5). The PL intensity of modified $MoS_2$ regions is significantly reduced. The imaging was performed with an excitation wavelength of 488 nm. (c) PL intensity of modified and unmodified $MoS_2$ regions, respectively, obtained in water at different pH (pH 3, pH 5.5, and pH 8). Consistent with previous reports,[55] the PL intensity of the unmodified $MoS_2$ layer inversely increases with the pH. (d) Raman spectra obtained from modified (red line) and unmodified (blue line) bilayer $MoS_2$ regions. The spectra are compared to the Raman spectrum of the reference $MoS_2$ that was not exposed to the solution for electrografting (black line). The whole spectra and the exact positions from which the spectra were taken are shown in SI Figure S8.

occurring on the edges and grain boundaries.[31,49] In 2D $MoS_2$, the edges of the crystal and the sulfur vacancies are sites where molybdenum atoms are in a (+IV) valence state, leaving them coordinately unsaturated. The $d_{xy}$ and $d_{x^2-y^2}$ orbitals of the molybdenum atoms located at the edges extend into the electrolyte and interact strongly with the molecules from the environment (electron-donor species). These sites are thus more reactive, resulting in higher heterogeneous electron transfer rates on the edges, grain boundaries and defects compared to the rest of the basal plane.[28] The activity of the $MoS_2$ basal plane depends as well on the efficiency of injecting the electrons into 2D material, which depends on the quality of the contact between the electrode and the 2D material,[50] the sheet resistance through the 2D layer, and the interconnection between the individual monocrystals.[30] It is, therefore, expected that the layer thickness and the local surface roughness will vary as well between the individual $MoS_2$ flakes, just as observed in Figure 2e.

The quality of the electrografted layer was also inspected at the nanoscale using high resolution transmission electron microscopy (HR-TEM). For that purpose, $MoS_2$ was transferred onto a metallized holey TEM grid and subjected to electrografting. SI Figure S4 shows HR-TEM images of suspended $MoS_2$ regions. Modified $MoS_2$ exhibits relatively uniform contrast at the scale of several hundreds of nanometers indicating homogeneous surface coverage with the electrografted layer.

For inspecting the selectivity of the method at the nanoscale, we performed TEM imaging on a device with three $MoS_2$ nanoribbons (Figure 3a) of which two of them were electrografted. The electrografting was performed on two ribbons by polarizing them cathodically, while the third ribbon was kept as a control and was not polarized. Both ribbons subjected to electrografting clearly exhibit an increased mass contrast in comparison to the control ribbon, indicating that the TFMB layer was selectively grafted only on the cathodically polarized nanoribbons. A comparison of the nanoribbons TEM


https://dx.doi.org/10.1021/acsanm.0c02628
ACS Appl. Nano Mater. 2021, 4, 1076−1084

image contrast before and after the deposition is presented in SI Figure S5. The difference in image contrast is further qualitatively assessed by plotting the mean intensity profile (Figure 3a, line plot) along with a narrow box (Figure 3a, blue box), revealing three distinct intensity levels that correspond to the $SiN_x$ membrane, the unmodified $MoS_2$, and the modified $MoS_2$. The observed contrast is relatively uniform along the inspected part of the nanoribbon surface indicating that at the scale of several hundreds of nanometers the entirety of the ribbon is homogeneously modified. The shortest distance between the unmodified and the modified ribbon is only about 300 nm, demonstrating the spatial selectivity of this modification method.

To additionally confirm the selectivity of the deposition, we performed an elemental analysis of the modified and the unmodified control $MoS_2$ ribbons. We utilized the energy-dispersive X-ray spectroscopy (EDX) in scanning TEM (STEM-EDX) mode. Figure 3b shows the EDX spectra from three different parts of the region indicated in Figure 3a. The high angle annular dark field STEM (HAADF-STEM) image of the inspected region is presented in Figure 3c (left) together with the EDX elemental maps. The EDX spectra and elemental maps reveal higher content of carbon and fluorine in the modified $MoS_2$ ribbon compared to the unmodified control ribbon, which originates from the $CF_3$-substituted aryl groups grafted on the surface. This is consistent with previous density functional theory calculations[21] showing that spontaneous grafting on pristine $MoS_2$ is energetically unfavorable. The comparison of fluorine signals can be found in SI Figure S6. The low-intensity fluorine peaks in EDX spectra of $SiN_x$ membrane and the $MoS_2$ unmodified control ribbon mainly originate from the fluorine chemistry process used in the device fabrication. This was additionally confirmed by comparing the EDX data of the device exposed to TFMB and the reference sample (SI Table S3).

After confirming the specificity and selectivity of the method at the nanoscale, we have proceeded with methods that allowed probing the uniformity of the electrografting on $MoS_2$ at large scale such as photoluminescence (PL) and Raman spectroscopy. Furthermore, we investigated the impact of electrografting on the performance of $MoS_2$ devices by performing electrical conductance measurements.

PL imaging was performed on devices with modified and unmodified $MoS_2$ in dry and aqueous conditions (Figure 4 and SI Figure S7). In all cases, we observe a dramatic reduction of PL intensity on all modified surfaces. So far, the exact mechanism responsible for PL reduction is not clear to us. Compared to unmodified $MoS_2$, the PL intensity of electrochemically grafted $MoS_2$ stays unaffected by pH changes in a range of pH 3−8 (Figure 4c), even after long exposure to the solution (~1 h). This indicates good protection of the $MoS_2$ surface by the film which is homogeneous, chemically inert, and strongly bonded to the $MoS_2$ surface.

As previously mentioned, it has been shown that cathodic polarization might induce the phase transition of $MoS_2$ from semiconducting 2H to the metallic 1T crystalline phase.[37,38] From HR-TEM characterization of electrografted layer on suspended $MoS_2$ (SI Figure S4c,d), it can be seen that the crystalline structure of electrografted $MoS_2$ stayed preserved. To additionally confirm that the metallization of $MoS_2$ did not occur, the Raman spectra were recorded on modified and unmodified $MoS_2$ regions, respectively. The spectra were also compared to the spectrum of a reference $MoS_2$ sample that was not exposed to TFMB solution. Figure 4d shows the region 300 $cm^{-1}$ - 480 $cm^{-1}$ with two prominent peaks that correspond to $E^1_{2g}$ (~384 $cm^{-1}$) and $A_{1g}$ (405 $cm^{-1}$) modes, respectively, and are characteristic for the 2H phase. None of the spectra exhibits signatures that would be associated with the 1T $MoS_2$ transition. The entire spectra and the exact positions from which the spectra were taken can be found in SI Figure S8a−c. Interestingly, compared to unmodified and reference $MoS_2$, we observe the broadening of $E^1_{2g}$ and $A_{1g}$ peaks in modified $MoS_2$ (SI Figure S8d). The broadening of these Raman modes in 2D TMDCs is associated with perturbation of in- and out-of-plane vibrations which can originate from the defects[51] or molecules bonded on the surface.[24] In this case, aryl groups that are electrografted on the $MoS_2$ surface disrupt the symmetry of the $MoS_2$ crystal, which affects in- and out-of-plane vibrations. A similar effect has been previously observed as well in nonelectrochemical grafting with diazonium salts on $MoS_2$[24] and graphene.[52]

The 2H crystalline phase was also confirmed by electrical conductance measurements of the $MoS_2$ nanoribbons in two-terminal configuration. We measured the conductances in dry conditions before and after the modification (SI Figure S9). The conductance values after the modification increased by approximately 1 order of magnitude (SI Figure S10). We observe similar conductance increase with control ribbons that were exposed to TFMB solution, and attribute this increase to physisorption of aromatic molecules on $MoS_2$.[53] Since the expected conductance increase due to metallization is about 7 orders of magnitude,[54] it can be concluded that the phase transition did not occur during the electrochemical grafting process and that the 2H crystalline phase of $MoS_2$ stayed preserved.

## CONCLUSION

We have shown that the TFMB aryl-diazonium salt can be electrochemically grafted on the basal plane of 2D semiconducting $MoS_2$. Compared to the majority of previously reported $MoS_2$ chemical modification methods, this approach is not limited to defective sites and does not require a $MoS_2$ phase transition. The electrografting occurs only on $MoS_2$ that is cathodically polarized, which can be exploited to selectively modify individually contacted regions. To demonstrate this ability at the nanoscale, we modified the surface of $MoS_2$ nanoribbons by addressing them individually via a different electrode. This approach paves the way for tailoring surface chemistry and optoelectronic properties of individual 2D TMDCs nanostructures that are in close proximity to each other. In biosensing, a specific functionalization of neighboring nanoribbons with different bioreceptors could increase the sensing capabilities of such 2D material-based sensors.[56,57] Sensing devices that rely on the ionic and electronic in-plane current measurement through nanopores in 2D materials[4] could as well take advantage of this approach by engineering specific interactions between the nanopore and the analyte. As chemical agents, diazonium salts are especially suitable for electrografting since they can be easily reduced, and most importantly, they offer the possibility of introducing a wide variety of different functional groups on the material's surface. The same strategy could be potentially applicable as well to other 2D semiconducting materials that can act as an electrode in the same potential window in which the electrochemical reduction of aryl diazonium salts occurs. We believe that such electrochemically activated reaction offers additional control in


https://dx.doi.org/10.1021/acsanm.0c02628
ACS Appl. Nano Mater. 2021, 4, 1076−1084

nanomaterial engineering and advances existing capabilities in fabrication of future nanoelectronic devices.

## EXPERIMENTAL SECTION

All the reagents and solvents used were analytical grade and purchased from Sigma − Aldrich, Merck, Darmstadt, Germany.

**$MoS_2$ Transfer.** 2D $MoS_2$ mono- and bilayers were grown by metal organic chemical vapor deposition on sapphire and characterized as reported previously.[41] The layer thickness was confirmed by optical contrast and AFM measurements. Monocrystals were transferred onto the target substrate by wet transfer method described elsewhere.[58]

**$MoS_2$ Devices.** After the $MoS_2$ transfer and cleaning, electron beam lithography (EBL) and electron beam assisted metal evaporation was used to pattern and evaporate the electrodes (5 nm Ti/70 nm Au/5 nm Pt) to contact $MoS_2$ layers.

**Devices with $MoS_2$ Nanoribbons on $SiN_x$ Membrane.** The protocol for the fabrication process is available elsewhere.[4,58] In short, prior to $MoS_2$ transfer, we created 30 $\mu$m × 30 $\mu$m SiNx membrane with an aperture by using photolithography, EBL, fluorine-based ($C_2F_6$) reactive ion etching (RIE), and wet etching in a hot potassium hydroxide solution (30% w/w). After the $MoS_2$ transfer and cleaning, EBL and metal evaporation were used to pattern and evaporate the electrodes (5 nm Ti/70 nm Au/5 nm Pt) on top of the $MoS_2$. After patterning these contacts, the $MoS_2$ monolayer is etched into nanoribbons (2 $\mu$m × 500 nm) using EBL and RIE ($O_2$ plasma). In all EBL steps, a three-step alignment scheme was used to achieve the necessary precision between individual lithographic steps. Before electrografting, the devices were rinsed with acetone and isopropanol, and carefully dried with a stream of nitrogen. Each device was fixed to a PCB board, the electrodes were wire-bonded to the PCB contacts serving to connect the electrodes to a potentiostat.

**$MoS_2$ Suspended on TEM Grids.** First, a thin metal coating (5 nm Ti/70 nm Au/5 nm Pt) was evaporated on top of holey TEM silicon nitride grid (Norcada, Edmonton, Canada). The $MoS_2$ was then transferred over the micron sized openings in the metallized grid leaving the parts of $MoS_2$ freestanding. The grid was connected as a working electrode.

**Electrochemical Grafting.** Grafting was performed by cyclic voltammetry (CV) in a solution of 3,5-bis(trifluoromethyl)-benzenediazonium tetrafluoroborate, TFMB, (5 mM) in acetonitrile with tetrabutylammonium perchlorate, TBAP, (100 mM) which was used as a supporting electrolyte. Details on the synthesis and characterization of TFMB can be found in the SI. A three-electrode setup was employed, with a $MoS_2$ nanoribbon working electrode, a Pt-wire counter electrode and a double-junction Ag|AgCl|3 M KCl reference electrode (BASinc, West Lafayette, IN) connected to the PalmSens2 potentiostat (Palm Instruments BV, Houten, Netherlands). All electrografting experiments were performed at 5 °C under dimmed light. The $MoS_2$ nanoribbon electrode was polarized between +450 mV and −750 mV at 50 mV $s^{-1}$ during five cycles. After deposition, the electrodes and the devices were thoroughly rinsed with acetonitrile, and gently dried with a nitrogen flow.

**Atomic Force Microscopy.** The devices and substrates were imaged using microcantilevers (70 kHz, 2 N $m^{-1}$, Olympus) and an atomic force microscope Asylum Cypher (Oxford Instruments−Asylum Research, Santa Barbara, CA) operating in tapping (AC) mode. The theoretical height of TFMB monolayer covalently bonded to $MoS_2$ was calculated from the molecular structure in Avogadro software and estimated to be 6.1 Å. The measured height of the layer will be higher due to the interactions of the molecules with the AFM tip.

**Scanning/Transmission Electron Microscopy.** BF-TEM and HAADF-STEM images of the devices were acquired using a Talos TEM, (ThermoFisher Scientific, Hillsboro, OR) operated at an accelerating voltage of 80 kV, which is below the electron-beam induced knock-on damage of $MoS_2$. EDX elemental maps were recorded in the same microscope in STEM mode by collecting characteristic X-ray signals using two silicon-drift in-column detectors. The EDX data were processed and fitted with Velox software (ThermoFisher Scientific, Hillsboro, OR).

**Photoluminescence (PL) Imaging.** Photoluminescence images of $MoS_2$ flakes were taken by epifluorescence microscopy on an inverted microscope (IX71, Olympus, Tokyo, Japan). A 488 nm laser (Sapphire, Coherent) was used to excite $MoS_2$ with a widefield illumination at a power density of 19 W/$cm^2$. The emission from the sample passes an emission filter (StopLine 405/488/568, Semrock, IDEX Corporation, United States) before imaged by an EMCCD camera (iXon Du-897, Andor Technology, Oxford Instruments, United Kingdom). The PL images are averaged over 1000 frames with exposure time of 50 ms. The PL of the sample was measured first in ambient air, and then in solution. The pH of a solution was adjusted by adding a small amount of HCl or KOH, respectively.

**Raman Spectroscopy.** The measurements were performed using Ranishaw inVia Confocal Raman Microscope operating at 532 nm for excitation and with a laser power of 0.5 mW. A diffraction grating of 3000 $mm^{-1}$ was used. The spot size was ∼1 $\mu$m. Each spectrum was recorded by accumulating three scans. The exposure time for each spectrum was 10 s.

**Conductance Measurements in Dry Conditions.** The conductance measurements of contacted $MoS_2$ ribbons were performed by measuring I−V characteristics in a two-terminal configuration in air and at room temperature.

## ASSOCIATED CONTENT

### Supporting Information

The Supporting Information is available free of charge at https://pubs.acs.org/doi/10.1021/acsanm.0c02628.

Aryl-diazonium salt synthesis and characterization, AFM, XPS, TEM, EDX, Photoluminescence, Raman spectroscopy, Conductance measurements (PDF)

## AUTHOR INFORMATION


### Corresponding Authors

**Martina Lihter** − *Laboratory of Nanoscale Biology, Institute of Bioengineering, School of Engineering, EPFL, 1015 Lausanne, Switzerland;* orcid.org/0000-0003-1859-8453; Email: martina.lihter@epfl.ch

**Aleksandra Radenovic** − *Laboratory of Nanoscale Biology, Institute of Bioengineering, School of Engineering, EPFL, 1015 Lausanne, Switzerland;* orcid.org/0000-0001-8194-2785; Email: aleksandra.radenovic@epfl.ch

### Authors

**Michael Graf** − *Laboratory of Nanoscale Biology, Institute of Bioengineering, School of Engineering, EPFL, 1015 Lausanne, Switzerland;* orcid.org/0000-0001-6201-7471

**Damir Iveković** − *Laboratory of General and Inorganic Chemistry and Electroanalysis, Faculty of Food Technology and Biotechnology, University of Zagreb, 10 000 Zagreb, Croatia*

**Miao Zhang** − *Laboratory of Nanoscale Biology, Institute of Bioengineering, School of Engineering, EPFL, 1015 Lausanne, Switzerland*

**Tzu-Hsien Shen** − *Institute of Materials, EPFL, 1015 Lausanne, Switzerland*

**Yanfei Zhao** − *Laboratory of Nanoscale Electronics and Structures, Institute of Electrical Engineering, School of Engineering, EPFL, 1015 Lausanne, Switzerland*

**Michal Macha** − *Laboratory of Nanoscale Biology, Institute of Bioengineering, School of Engineering, EPFL, 1015 Lausanne, Switzerland*

**Vasiliki Tileli** − *Institute of Materials, EPFL, 1015 Lausanne, Switzerland;* orcid.org/0000-0002-0520-6900




https://dx.doi.org/10.1021/acsanm.0c02628
ACS Appl. Nano Mater. 2021, 4, 1076−1084

Complete contact information is available at:
https://pubs.acs.org/10.1021/acsanm.0c02628

### Author Contributions

M.L. initiated the idea, performed electrochemical grafting, AFM and TEM imaging. M.L., D.I., and A.R. designed the experiments. M.G. fabricated devices. D.I. proposed the type of diazonium salt used, performed the synthesis and FTIR characterization, and participated in the final reviewing and editing of the manuscript. T.-H.S. performed EDX measurements under V.T supervision. M.Z. performed PL imaging. Y.Z. synthesized $MoS_2$ material and performed Raman spectroscopy measurements. M.M. synthesized continuous $MoS_2$ material. A.R. supervised the research. M.L. and M.G. wrote the manuscript with the comments of all the coauthors.

### Notes

The authors declare no competing financial interest.

## ■ ACKNOWLEDGMENTS

We thank Prof. Carlotta Guiducci for providing access to a potentiostat, Prof. Andras Kis for the access to AFM and probe-station, and Dr. Ahmet Avsar for useful discussions. We thank Dr. Pierre Mettraux and Molecular and Hybrid Materials Characterization Center at EPFL for XPS measurements. This work was financially supported by the Swiss National Science Foundation (SNSF) Consolidator grant (BIONIC BSCGI0_157802) and CCMX project ("Large Area Growth of 2D Materials for device integration"). T.-H.S. and V.T. acknowledge support by the Swiss National Science Foundation (SNSF) under award no. 200021_175711.

## ■ REFERENCES

(1) Radisavljevic, B.; Radenovic, A.; Brivio, J.; Giacometti, V.; Kis, A. Single-Layer MoS2 Transistors. *Nat. Nanotechnol.* **2011**, *6* (3), 147−150.
(2) Gonzalez Marin, J. F.; Unuchek, D.; Watanabe, K.; Taniguchi, T.; Kis, A. MoS2 Photodetectors Integrated with Photonic Circuits. *npj 2D Mater. Appl.* **2019**, *3* (1), 14.
(3) Sarkar, D.; Liu, W.; Xie, X.; Anselmo, A. C.; Mitragotri, S.; Banerjee, K. MoS2 Field-Effect Transistor for next-Generation Label-Free Biosensors. *ACS Nano* **2014**, *8* (4), 3992−4003.
(4) Graf, M.; Lihter, M.; Altus, D.; Marion, S.; Radenovic, A. Transverse Detection of DNA Using a $MoS_2$ Nanopore. *Nano Lett.* **2019**, *19* (12), 9075−9083.
(5) Feng, J.; Graf, M.; Liu, K.; Ovchinnikov, D.; Dumcenco, D.; Heiranian, M.; Nandigana, V.; Aluru, N. R.; Kis, A.; Radenovic, A. Single-Layer MoS2 Nanopores as Nanopower Generators. *Nature* **2016**, *536* (7615), 197−200.
(6) Graf, M.; Lihter, M.; Unuchek, D.; Sarathy, A.; Leburton, J.-P.; Kis, A.; Radenovic, A. Light Enhanced Blue Energy Generation Using MoS2 Nanopores. *Joule* **2019**, *3*, 1−16.
(7) Huang, J.; Wei, Z.; Liao, J.; Ni, W.; Wang, C.; Ma, J. Molybdenum and Tungsten Chalcogenides for Lithium/Sodium-Ion Batteries: Beyond MoS 2. *J. Energy Chem.* **2019**, *33*, 100−124.
(8) Manzeli, S.; Ovchinnikov, D.; Pasquier, D.; Yazyev, O. V.; Kis, A. 2D Transition Metal Dichalcogenides. *Nat. Rev. Mater.* **2017**, *2* (8), 17033.
(9) Bertolazzi, S.; Gobbi, M.; Zhao, Y.; Backes, C.; Samorì, P. Molecular Chemistry Approaches for Tuning the Properties of Two-Dimensional Transition Metal Dichalcogenides. *Chem. Soc. Rev.* **2018**, *47* (17), 6845−6888.
(10) Luo, P.; Zhuge, F.; Zhang, Q.; Chen, Y.; Lv, L.; Huang, Y.; Li, H.; Zhai, T. Doping Engineering and Functionalization of Two-Dimensional Metal Chalcogenides. *Nanoscale Horizons* **2019**, *4* (1), 26−51.
(11) Li, H.; Tsai, C.; Koh, A. L.; Cai, L.; Contryman, A. W.; Fragapane, A. H.; Zhao, J.; Han, H. S.; Manoharan, H. C.; Abild-Pedersen, F.; Nørskov, J. K.; Zheng, X. Activating and Optimizing MoS2 Basal Planes for Hydrogen Evolution through the Formation of Strained Sulphur Vacancies. *Nat. Mater.* **2016**, *15* (1), 48−53.
(12) Li, G.; Zhang, D.; Qiao, Q.; Yu, Y.; Peterson, D.; Zafar, A.; Kumar, R.; Curtarolo, S.; Hunte, F.; Shannon, S.; Zhu, Y.; Yang, W.; Cao, L. All the Catalytic Active Sites of MoS2 for Hydrogen Evolution. *J. Am. Chem. Soc.* **2016**, *138* (51), 16632−16638.
(13) Ouyang, Y.; Ling, C.; Chen, Q.; Wang, Z.; Shi, L.; Wang, J. Activating Inert Basal Planes of MoS2 for Hydrogen Evolution Reaction through the Formation of Different Intrinsic Defects. *Chem. Mater.* **2016**, *28* (12), 4390−4396.
(14) Makarova, M.; Okawa, Y.; Aono, M. Selective Adsorption of Thiol Molecules at Sulfur Vacancies on MoS 2(0001), Followed by Vacancy Repair via S-C Dissociation. *J. Phys. Chem. C* **2012**, *116* (42), 22411−22416.
(15) Bertolazzi, S.; Bonacchi, S.; Nan, G.; Pershin, A.; Beljonne, D.; Samorì, P. Engineering Chemically Active Defects in Monolayer MoS2Transistors via Ion-Beam Irradiation and Their Healing via Vapor Deposition of Alkanethiols. *Adv. Mater.* **2017**, *29* (18), n/a−n/a.
(16) Presolski, S.; Pumera, M. Covalent Functionalization of MoS2. *Mater. Today* **2016**, *19* (3), 140−145.
(17) Chou, S. S.; De, M.; Kim, J.; Byun, S.; Dykstra, C.; Yu, J.; Huang, J.; Dravid, V. P. Ligand Conjugation of Chemically Exfoliated MoS2. *J. Am. Chem. Soc.* **2013**, *135* (12), 4584−4587.
(18) Liu, T.; Wang, C.; Gu, X.; Gong, H.; Cheng, L.; Shi, X.; Feng, L.; Sun, B.; Liu, Z. Drug Delivery with PEGylated MoS2 Nano-Sheets for Combined Photothermal and Chemotherapy of Cancer. *Adv. Mater.* **2014**, *26* (21), 3433−3440.
(19) Tuxen, A.; Kibsgaard, J.; Gøbel, H.; Lægsgaard, E.; Topsøe, H.; Lauritsen, J. V.; Besenbacher, F. Size Threshold in the Dibenzothiophene Adsorption on MoS2 Nanoclusters. *ACS Nano* **2010**, *4* (8), 4677−4682.
(20) Wang, T.; Zhu, R.; Zhuo, J.; Zhu, Z.; Shao, Y.; Li, M. Direct Detection of DNA below Ppb Level Based on Thionin-Functionalized Layered MoS2 Electrochemical Sensors. *Anal. Chem.* **2014**, *86* (24), 12064−12069.
(21) Chu, X. S.; Yousaf, A.; Li, D. O.; Tang, A. A.; Debnath, A.; Ma, D.; Green, A. A.; Santos, E. J. G.; Wang, Q. H. Direct Covalent Chemical Functionalization of Unmodified Two-Dimensional Molybdenum Disulfide. *Chem. Mater.* **2018**, *30* (6), 2112−2128.
(22) Backes, C.; Berner, N. C.; Chen, X.; Lafargue, P.; LaPlace, P.; Freeley, M.; Duesberg, G. S.; Coleman, J. N.; McDonald, A. R. Functionalization of Liquid-Exfoliated Two-Dimensional 2H-MoS2. *Angew. Chem., Int. Ed.* **2015**, *54* (9), 2638−2642.
(23) Vera-Hidalgo, M.; Giovanelli, E.; Navío, C.; Pérez, E. M. Mild Covalent Functionalization of Transition Metal Dichalcogenides with Maleimides: A "Click" Reaction for 2H-MoS 2 and WS 2. *J. Am. Chem. Soc.* **2019**, *141* (9), 3767−3771.
(24) Voiry, D.; Goswami, A.; Kappera, R.; Silva, C. de C. C. e; Kaplan, D.; Fujita, T.; Chen, M.; Asefa, T.; Chhowalla, M. Covalent Functionalization of Monolayered Transition Metal Dichalcogenides by Phase Engineering. *Nat. Chem.* **2015**, *7* (1), 45−49.
(25) Knirsch, K. C.; Berner, N. C.; Nerl, H. C.; Cucinotta, C. S.; Gholamvand, Z.; McEvoy, N.; Wang, Z.; Abramovic, I.; Vecera, P.; Halik, M.; Sanvito, S.; Duesberg, G. S.; Nicolosi, V.; Hauke, F.; Hirsch, A.; Coleman, J. N.; Backes, C. Basal-Plane Functionalization of Chemically Exfoliated Molybdenum Disulfide by Diazonium Salts. *ACS Nano* **2015**, *9* (6), 6018−6030.
(26) Tuci, G.; Mosconi, D.; Rossin, A.; Luconi, L.; Agnoli, S.; Righetto, M.; Pham-Huu, C.; Ba, H.; Cicchi, S.; Granozzi, G.; Giambastiani, G. Surface Engineering of Chemically Exfoliated MoS2 in a "Click": How to Generate Versatile Multifunctional Transition Metal Dichalcogenides-Based Platforms. *Chem. Mater.* **2018**, *30* (22), 8257−8269.
(27) Yan, E. X.; Cabán-Acevedo, M.; Papadantonakis, K. M.; Brunschwig, B. S.; Lewis, N. S. Reductant-Activated, High-Coverage,

Covalent Functionalization of 1T′-MoS2. *ACS Mater. Lett.* **2020**, *2* (2), 133−139.
(28) Ahmed, S. M.; Gerischer, H. Influence of Crystal Surface Orientation on Redox Reactions at Semiconducting MoS2. *Electrochim. Acta* **1979**, *24* (6), 705−711.
(29) Ahmed, S. M. Surface and Photoelectrochemical Studies of Semiconducting MoS2. *Electrochim. Acta* **1982**, *27* (6), 707−712.
(30) Henrotte, O.; Bottein, T.; Casademont, H.; Jaouen, K.; Bourgeteau, T.; Campidelli, S.; Derycke, V.; Jousselme, B.; Cornut, R. Electronic Transport of MoS2Monolayered Flakes Investigated by Scanning Electrochemical Microscopy. *ChemPhysChem* **2017**, *18* (19), 2777−2781.
(31) Ritzert, N. L.; Szalai, V. A.; Moffat, T. P. Mapping Electron Transfer at MoS2 Using Scanning Electrochemical Microscopy. *Langmuir* **2018**, *34* (46), 13864−13870.
(32) Delamar, M.; Hitmi, R.; Pinson, J.; Savéant, J. Covalent Modification of Carbon Surfaces by Grafting of Functionalized Aryl Radicals Produced from Electrochemical Reduction of Diazonium Salts. *J. Am. Chem. Soc.* **1992**, *114* (14), 5883−5884.
(33) Henry De Villeneuve, C.; Pinson, J.; Bernard, M. C.; Allongue, P. Electrochemical Formation of Close-Packed Phenyl Layers on Si(111). *J. Phys. Chem. B* **1997**, *101* (14), 2415−2420.
(34) Pinson, J.; Podvorica, F. Attachment of Organic Layers to Conductive or Semiconductive Surfaces by Reduction of Diazonium Salts. *Chem. Soc. Rev.* **2005**, *34* (5), 429−439.
(35) Hunger, R.; Jaegermann, W.; Merson, A.; Shapira, Y.; Pettenkofer, C.; Rappich, J. Electronic Structure of Methoxy-, Bromo-, and Nitrobenzene Grafted onto Si(111). *J. Phys. Chem. B* **2006**, *110* (31), 15432−15441.
(36) Paulus, G. L. C.; Wang, Q. H.; Strano, M. S. Covalent Electron Transfer Chemistry of Graphene with Diazonium Salts. *Acc. Chem. Res.* **2013**, *46* (1), 160−170.
(37) Wu, S.; Zeng, Z.; He, Q.; Wang, Z.; Wang, S. J.; Du, Y.; Yin, Z.; Sun, X.; Chen, W.; Zhang, H. Electrochemically Reduced Single-Layer MoS2 Nanosheets: Characterization, Properties, and Sensing Applications. *Small* **2012**, *8* (14), 2264−2270.
(38) Chia, X.; Ambrosi, A.; Sedmidubský, D.; Sofer, Z.; Pumera, M. Precise Tuning of the Charge Transfer Kinetics and Catalytic Properties of MoS 2 Materials via Electrochemical Methods. *Chem. - Eur. J.* **2014**, *20* (52), 17426−17432.
(39) Nasir, M. Z. M.; Sofer, Z.; Ambrosi, A.; Pumera, M. A Limited Anodic and Cathodic Potential Window of MoS2: Limitations in Electrochemical Applications. *Nanoscale* **2015**, *7* (7), 3126−3129.
(40) Menanteau, T.; Levillain, E.; Downard, A. J.; Breton, T. Evidence of Monolayer Formation via Diazonium Grafting with a Radical Scavenger: Electrochemical, AFM and XPS Monitoring. *Phys. Chem. Chem. Phys.* **2015**, *17* (19), 13137−13142.
(41) Cun, H.; Macha, M.; Kim, H. K.; Liu, K.; Zhao, Y.; LaGrange, T.; Kis, A.; Radenovic, A. Wafer-Scale MOCVD Growth of Monolayer MoS2 on Sapphire and SiO2. *Nano Res.* **2019**, *12* (10), 2646−2652.
(42) Li, Y.; Zhou, Z.; Zhang, S.; Chen, Z. MoS2 Nanoribbons: High Stability and Unusual Electronic and Magnetic Properties. *J. Am. Chem. Soc.* **2008**, *130* (49), 16739−16744.
(43) Li, Y.; Moy, E. C.; Murthy, A. A.; Hao, S.; Cain, J. D.; Hanson, E. D.; DiStefano, J. G.; Chae, W. H.; Li, Q.; Wolverton, C.; Chen, X.; Dravid, V. P. Large-Scale Fabrication of MoS2 Ribbons and Their Light-Induced Electronic/Thermal Properties: Dichotomies in the Structural and Defect Engineering. *Adv. Funct. Mater.* **2018**, *28* (13), 1−9.
(44) Chen, S.; Kim, S.; Chen, W.; Yuan, J.; Bashir, R.; Lou, J.; Van Der Zande, A. M.; King, W. P. Monolayer MoS 2 Nanoribbon Transistors Fabricated by Scanning Probe Lithography. *Nano Lett.* **2019**, *19* (3), 2092−2098.
(45) Combellas, C.; Jiang, D. E.; Kanoufi, F.; Pinson, J.; Podvorica, F. I. Steric Effects in the Reaction of Aryl Radicals on Surfaces. *Langmuir* **2009**, *25* (1), 286−293.
(46) Bélanger, D.; Pinson, J. Electrografting: A Powerful Method for Surface Modification. *Chem. Soc. Rev.* **2011**, *40* (7), 3995−4048.
(47) and, R. N.; Heintz, A.; Niesner, R.; Heintz, A. Diffusion Coefficients of Aromatics in Aqueous Solution. *J. Chem. Eng. Data* **2000**, *45* (6), 1121−1124.
(48) Mathivanan, N.; Johnston, L. J.; Wayner, D. D. M. Photochemical Generation of Radical Anions of Photolabile Aryl Ketones. *J. Phys. Chem.* **1995**, *99* (20), 8190−8195.
(49) Tan, S. M.; Ambrosi, A.; Sofer, Z.; Huber, Š.; Sedmidubský, D.; Pumera, M. Pristine Basal- and Edge-Plane-Oriented Molybdenite MoS 2 Exhibiting Highly Anisotropic Properties. *Chem. - Eur. J.* **2015**, *21* (19), 7170−7178.
(50) Voiry, D.; Fullon, R.; Yang, J.; de Carvalho Castro e Silva, C.; Kappera, R.; Bozkurt, I.; Kaplan, D.; Lagos, M. J.; Batson, P. E.; Gupta, G.; Mohite, A. D.; Dong, L.; Er, D.; Shenoy, V. B.; Asefa, T.; Chhowalla, M. The Role of Electronic Coupling between Substrate and 2D MoS2 Nanosheets in Electrocatalytic Production of Hydrogen. *Nat. Mater.* **2016**, *15* (9), 1003−1009.
(51) Mignuzzi, S.; Pollard, A. J.; Bonini, N.; Brennan, B.; Gilmore, I. S.; Pimenta, M. A.; Richards, D.; Roy, D. Effect of Disorder on Raman Scattering of Single-Layer MoS2. *Phys. Rev. B: Condens. Matter Mater. Phys.* **2015**, *91* (19), 195411.
(52) Sharma, R.; Baik, J. H.; Perera, C. J.; Strano, M. S. Anomalously Large Reactivity of Single Graphene Layers and Edges toward Electron Transfer Chemistries. *Nano Lett.* **2010**, *10* (2), 398−405.
(53) Wang, Y.; Slassi, A.; Stoeckel, M.; Bertolazzi, S.; Cornil, J.; Beljonne, D.; Samorì, P. Doping of Monolayer Transition-Metal Dichalcogenides via Physisorption of Aromatic Solvent Molecules. *J. Phys. Chem. Lett.* **2019**, *10* (3), 540−547.
(54) Acerce, M.; Voiry, D.; Chhowalla, M. Metallic 1T Phase MoS2 Nanosheets as Supercapacitor Electrode Materials. *Nat. Nanotechnol.* **2015**, *10* (4), 313−318.
(55) Zhang, W.; Matsuda, K.; Miyauchi, Y. PH-Dependent Photoluminescence Properties of Monolayer Transition-Metal Dichalcogenides Immersed in an Aqueous Solution. *J. Phys. Chem. C* **2018**, *122* (24), 13175−13181.
(56) Lee, J.; Dak, P.; Lee, Y.; Park, H.; Choi, W.; Alam, M. A.; Kim, S. Two-Dimensional Layered MoS 2 Biosensors Enable Highly Sensitive Detection of Biomolecules. *Sci. Rep.* **2015**, *4*, 1−7.
(57) Lee, D.-W.; Lee, J.; Sohn, I. Y.; Kim, B.-Y.; Son, Y. M.; Bark, H.; Jung, J.; Choi, M.; Kim, T. H.; Lee, C.; Lee, N.-E. Field-Effect Transistor with a Chemically Synthesized MoS2 Sensing Channel for Label-Free and Highly Sensitive Electrical Detection of DNA Hybridization. *Nano Res.* **2015**, *8* (7), 2340−2350.
(58) Graf, M.; Lihter, M.; Thakur, M.; Georgiou, V.; Topolancik, J.; Ilic, B. R. R.; Liu, K. K.; Feng, J.; Astier, Y.; Radenovic, A. Fabrication and Practical Applications of Molybdenum Disulfide Nanopores. *Nat. Protoc.* **2019**, *14* (4), 1130−1168.


https://dx.doi.org/10.1021/acsanm.0c02628
*ACS Appl. Nano Mater.* 2021, 4, 1076−1084